Letter

M center in 4*H*-SiC is a carbon self-interstitial

J. Coutinho,[1,*] J. D. Gouveia,[1,†] T. Makino,[2] T. Ohshima,[2] Ž. Pastuović,[3] L. Bakrač,[4] T. Brodar,[4] and I. Capan[4]

[1]*I3N, Department of Physics, University of Aveiro, Campus Santiago, 3810-193 Aveiro, Portugal*

[2]*Takasaki Advanced Radiation Research Institute, National Institutes for Quantum and Radiological Science and Technology, 1233 Watanuki, Takasaki, Gunma 370-1292, Japan*

[3]*Centre for Accelerator Science, Australian Nuclear Science and Technology Organisation, 1 New Illawarra Rd, Lucas Heights, NSW 2234, Australia*

[4]*Ruđer Bošković Institute, Bijenicka 54, 10000 Zagreb, Croatia*

(Received 1 April 2021; accepted 7 May 2021; published 28 May 2021)

The list of semiconductor materials with spectroscopically fingerprinted self-interstitials is very short. The *M* center in 4*H*-SiC, a bistable defect responsible for a family of electron traps, has been deprived of a model which could unveil its real importance for almost two decades. Using advanced first-principles calculations and junction spectroscopy, we demonstrate that the properties of M, including bistability, annealing, reconfiguration kinetics, and electronic levels match those of the carbon self-interstitial.

DOI: 10.1103/PhysRevB.103.L180102

The identification of self-interstitials in technological crystalline materials constitutes a rare event with profound repercussions on several fields. Together with vacancies, they form a fundamental couple playing a central role in many properties and processes, including mass transport, crystal growth, doping, and countless solid-state reactions.

Silicon carbide, in particular its 4*H* polytype (4*H*-SiC), is a mainstream wide-gap semiconductor for power electronics [1,2] and a host for some of the most promising defects for quantum technologies [3–6]. In n-type material, while both Si and C vacancies have well-established spectroscopic signals accompanied by detailed models [7–13], little is known about the interstitials, apart from indirect findings from their interaction with vacancies [14,15] and some conjectural assignments. Deep Level Transient Spectroscopy (DLTS) peaks $EH_{1/3}$ [16,17], M [18,19], and EB [20] were to some extent related to carbon interstitials, but when the data are confronted to existing models [21–23], we only obtain a partial match. This contrasts with p-type SiC, where the connection of electron paramagnetic resonance signals T5 [24], EI1 and EI3 [25] to carbon self-interstitials finds support from first-principles calculations of hyperfine splitting constants, zero-field coupling coefficients [26], and *g*-tensor elements [27]. Of course, having reliable fingerprints of self-interstitials in 4*H*-SiC, and particularly in n-type material which offers better doping yield than p-type 4*H*-SiC, would improve our ability to control many defect engineering processes. For instance, an efficient production of quantum technological defects in n-type 4*H*-SiC (mostly vacancy related and invariably introduced by ion-implantation or irradiation techniques) strongly depends on our ability to control their annihilation on capturing self-interstitials during subsequent thermal treatments. This can only be achieved if we are able to follow the defects involved.

Below we demonstrate that the carbon self-interstitial (C_i) is responsible for a family of DLTS traps, attributed nearly two decades ago to a defect labeled '*M*'. They show up in irradiated n-type material after moderate annealing ($T \sim 200$°C) [18,19], including after irradiation with low-energy electrons (200 keV) [20], implying a relation to a carbon sublattice defect [28].

The *M* center is a bistable defect whose configuration is bias dependent. Spectrum labeled A, evidencing traps M_1 ($E_c - 0.42$ eV), and M_3 ($\sim E_c - 0.83$ eV) is obtained when the sample is cooled from room temperature under reverse bias. Conversely, when the DLTS scan is preceded by a gentle annealing at $T > 140$°C without bias, spectrum B appears, consisting of a single emission M_2 ($E_c - 0.63$ eV) [18,19]. The spectra can be cycled without loss of signal amplitude by repeatedly (un)biasing/annealing the sample. Since the M-peaks overlap with other prominent traps in irradiated 4*H*-SiC, namely $Z_{1/2}$ [29] and $S_{1/2}$ [30], the analysis must be carried out from differential spectra.

By applying isothermal heat treatments, it was possible to extract activation energies for the conversion between A and B configurations. In unbiased samples, the $B^=$ ground state builds up at the expense of metastable $A^=$ with an activation energy of 1.4 eV. The superscripts refer to the double minus charge state of the defect. Conversely, in reverse biased samples, the A^- state recovers from metastable B^- with an activation energy of 0.9 eV [18].

The reconfiguration within the neutral state could not be monitored because the B signal consisted of M_2 only ($B^= \rightarrow B^- + e^-$). It was argued that above room temperature, a fast conversion from B^- to A^- frustrated the observation of an expected M_4 peak related to $B^- \rightarrow B^0 + e^-$, effectively channeling any second emission through $A^- \rightarrow A^0 + e^-$ [19].

Besides complying with the above observations, we show that C_i features a rich set of properties that meet those of the *M* center, such as charge states and annealing. The model, developed using accurate range-separated hybrid density functional

*jose.coutinho@ua.pt

†Present address: CICECO, Department of Chemistry, University of Aveiro, Campus Santiago, 3810-193 Aveiro, Portugal.

 ©2021 American Physical Society

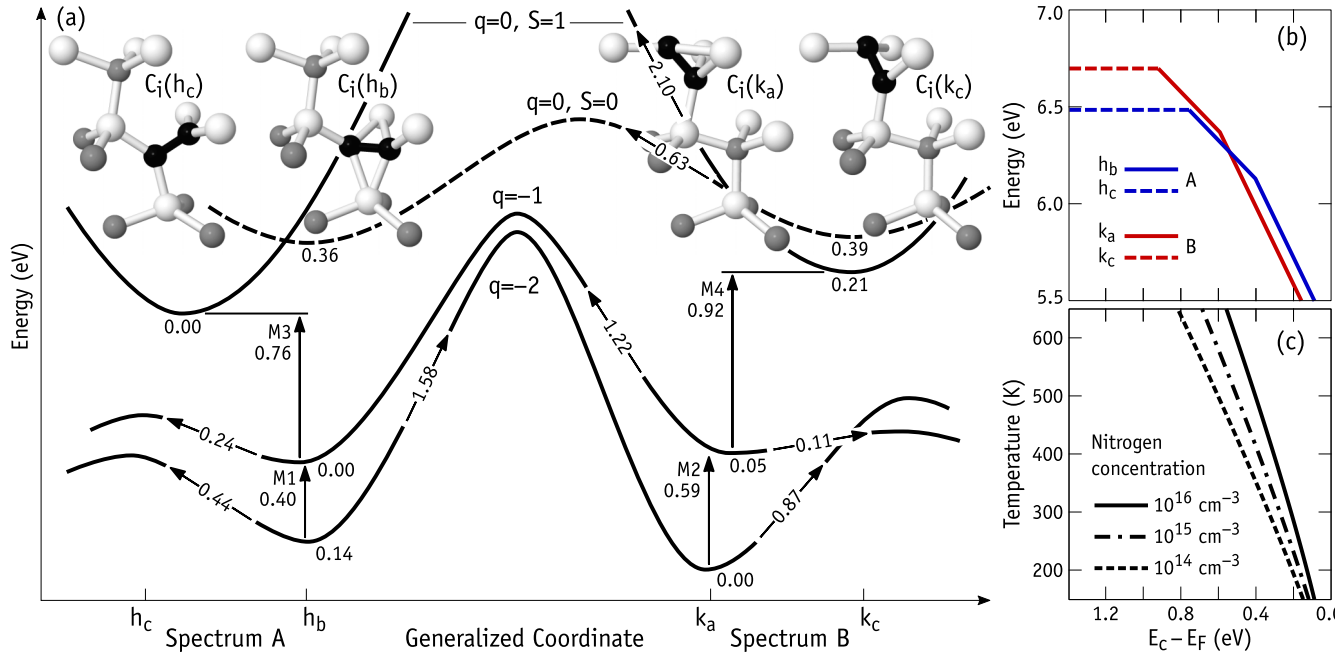

FIG. 1. (a) Atomistic structures and CCD for the C_i defect in n-type 4*H*-SiC for charge states $q = 0, -1$, and -2. Si and C neighbors are shown in white and gray, respectively. The C-dumbbell atoms are shown in black. Energies indicated below each potential minimum are relative to the ground state of that charge state. Energy barriers are relative to the structure of departure. (b) Formation energy diagram of C_i in n-type 4*H*-SiC. Energies of configurations A and B are shown in blue and red, respectively. Dashed lines stand for spin-1 states. (c) Temperature dependence of the Fermi level in n-type 4*H*-SiC for three values of nitrogen concentration.

calculations combined with junction spectroscopy, includes a detailed configuration coordinate diagram (CCD).

The electronic structure calculations were based on the plane wave/projector-augmented wave formalism [31] using the Vienna *Ab initio* Simulation Package [32,33], where plane waves with a cut-off energy of 420 eV described the Kohn-Sham wave functions. Total energies of stable and saddle-point structures were evaluated using the density functional proposed by Heyd, Scuseria, and Ernzerhof (HSE06) [34]. Defects were inserted in 400-atom 4*H*-SiC hexagonal supercells whose Brillouin zones (BZ) were integrated at $\mathbf{k} = \Gamma$. Forces on atoms were calculated within a semilocal approximation to the exchange-correlation interactions [35] and a BZ sampling grid of $2 \times 2 \times 2$ **k**-points. This allowed for the investigation of stable defect structures, transformation, and migration mechanisms. For the mechanisms, we used the climbing image nudged elastic band (NEB) method [36]. All forces were kept below 0.01 eV/Å. Formation energies as a function of the Fermi level were found by the usual method [37]. Spurious periodic effects were mitigated by adding a correction to the energies of charged supercells [38]. For further details and testing, see Refs. [39,40].

Experiments were carried out on Schottky diodes fabricated on 25-μm-thick n-type 4*H*-SiC layers (nitrogen doping up to 4.5×10^{14} cm^{-3}). They were pattern-implanted through their nickel Schottky contacts with 2-MeV He ions with a fluence of 10^9 cm^{-2}. Conventional DLTS measurements were carried out in the temperature range 100–450 K. Reverse voltage, pulse voltage, and pulse width were $V_R = -4$ V, $V_P = 0$ V, and $t_P = 10$ ms, respectively. These conditions correspond to a depletion width of 1.7–3.5 μm, safely avoiding the ion-projected range (4.8 μm). In order to stabilize the spectra and monitor structural transformations during the measurements, we applied isothermal DLTS [41,42]. Here, 20-min-long capacitance transients were acquired at a sampling rate of 60 kHz, keeping the temperature of the samples within ± 0.05 K from a set-point in the range 280–340 K. Before quenching the diodes to the measurement temperature, the *M* centers were either set to configuration A or B by applying a -30 V reverse bias annealing at 340 K for 20 min, or annealing at 450 K for 20 min without bias, respectively.

The geometry and electronic state of C_i in 4*H*-SiC strongly depends on its sublattice location and net charge, q. We found four conspicuous configurations [see Fig. 1(a)], some of which are already known [21–23]. We refer to them by a sublattice site (k or h) and an index letter (a, b, or c) that stands for the alignment of the C-C dimer [highlighted in black in Fig. 1(a)].

Like the analogous defect in diamond [43], neutral C_i adopts a spin-1 state with threefold coordinated C atoms. Two stable structures, namely $C_i^0(h_c)$ and $C_i^0(k_c)$, are assigned to the potential minima labeled with $q = 0$, $S = 1$, represented by a solid line in the upper part of the CCD of Fig. 1(a). Diamagnetic S = 0 states are metastable, and they were found with h_b and k_c structures (dashed line in the CCD). Energies indicated below the potential minima are relative to the ground state of the respective charge state. The defect can trap up to two electrons via overcoordination of the dumbbell atoms. Negatively charged h_b and k_a (with $q = -1$ and $q = -2$) are now stable while other geometries become unstable. NEB calculations show that h_c and k_c structures are saddle points for rotation of k_a and h_b around the $\langle 0001 \rangle$ crystalline axis. The respective energy barriers are indicated in the CCD over

the arrows that seemingly follow the potential curves. Note that $C_i^-(k)$ and $C_i^-(h)$ have rotation barriers as low as 0.11 and 0.24 eV. They are expected to show an effective trigonal symmetry due to thermal motion, even at cryogenic temperatures.

Figure 1(b) shows the formation energy of C_i in 4*H*-SiC as a function of the Fermi level with respect to the conduction band bottom, $E_c - E_F$. It was calculated by assuming a C-rich crystal with the carbon chemical potential obtained from bulk diamond. For the sake of clarity, line styles are connected to specific geometries (see legend) and the range of E_F values span the upper half of the gap only. Besides a charge state-dependent structure, C_i finds its most favorable sublattice site depending on the location of the Fermi level. In n-type material (without external bias), the most stable state is $C_i^=(k_a)$, whereas if the Fermi level is brought toward midgap (reverse bias conditions), the ground state is $C_i^0(h_c)$. This behavior closely follows that of the *M* center and its spectra A and B, hereafter assigned to $C_i(h)$ and $C_i(k)$, respectively.

Although the charge of defects is not directly accessible by capacitance measurements, the lack of a Poole-Frenkel effect for the $M_{1\text{-}3}$ emissions indicates that they involve acceptor transitions [19]. Directly measured capture cross-sections of the shallower M_1 and M_2 traps were about $5 \times 10^{-17}\,\mathrm{cm}^2$, suggesting $(=/-)$ transitions. The cross-section of M_3 was two orders of magnitude larger, consistent with M_1 and M_3 being two consecutive electron emissions from the same structure (spectrum A). M_2 plus a conjectured (undetected) M_4 peak would account for the analogous transitions in spectrum B. Hence, the type and number of transitions conform with the assignment of C_i to M.

The *M* center anneals out in the temperature range 580-640 K according to first order kinetics at a rate of $1.5 \times 10^{13} \exp(-2\,\mathrm{eV}/k_B T)\,\mathrm{s}^{-1}$, suggesting a dissociation mechanism or capture by an abundant and close trap [19]. Figure 1(c) gives the calculated Fermi energy in 4*H*-SiC as a function of temperature for three different nitrogen doping levels. The horizontal axis matches that of the formation energy diagram in Fig. 1(b). Considering the doping concentration $1\text{–}2 \times 10^{15}\,\mathrm{cm}^{-3}$ of the samples in Ref. [19], we conclude that the annealing temperature range coincides with the Fermi level window for which C_i is in the single negative charge state. From NEB calculations we find that the barriers for migration of C_i^- along crystalline basal and axial directions are 1.8 and 2.2 eV, respectively, the latter being the highest of two jumps between consecutive sublattice sites and close to the measured activation energy for the annealing of the *M* center [19].

Let us now compare the charge state transition levels of C_i with those of the *M* center. The calculated figures are shown in Fig. 1(a). The energies next to the vertical arrows (in eV) stand for trap depths with respect to the conduction band bottom. Accordingly, $C_i(h)$ has second and first acceptor transitions calculated at $E_c - 0.40$ eV and $E_c - 0.76$ eV, very close to the measured transitions of spectrum A, namely M_1 ($E_c - 0.42$ eV) and M_3 ($E_c - 0.83$ eV). Analogously, for $C_i(k)$ we find second and first acceptor transitions at $E_c - 0.59$ eV and $E_c - 0.92$ eV. The former agrees well with M_2 ($E_c - 0.63$ eV) from spectrum B, while the latter anticipates the location of M_4. The calculated levels neglect any temperature effects. They differ from the measured activation energies by a capture barrier and an entropy contribution, usually ~0.1 eV. Hence, the agreement obtained is considered very good.

Besides the above, the calculated $C_i(h) \leftrightarrow C_i(k)$ conversion barriers further confirm that the *M* center in 4*H*-SiC is a carbon interstitial. Like the carbon vacancy [39], in order to travel between two equivalent lattice sites along the main crystalline axis, C_i must perform two types of jumps between consecutive sublattice configurations. The jump with lower barrier is represented in Fig. 1(a) and separates $C_i(h)$ from $C_i(k)$ structures. Calculated barrier heights of 1.58 and 1.22 eV were obtained for forward and backward jumps $C_i^=(h_b) \rightarrow C_i^=(k_a)$ and $C_i^-(h_b) \leftarrow C_i^-(k_a)$, respectively. Both mechanisms are exothermal, and the barriers are rather close to the A → B and A ← B conversion activation energies of 1.4 and 0.9 eV, measured without and with bias, respectively [18].

A decisive piece of evidence in the identification of the *M* center would be a direct observation of the M_4 transition accompanied by M_2. Figure 2(a) shows DLTS spectra of a 4*H*-SiC n-type sample implanted with 2 MeV He ions, measured after annealing at 340 K under reverse bias (spectrum A) and 450 K without bias (spectrum B). The latter is dominated by the $Z_{1/2}$ peak (carbon vacancy) [7,29], with relatively smaller contributions from S_1/S_2 (silicon vacancy) [13,30], and a less understood broad feature known as EH_4, recently connected to a superposition of different alignments of anisotropic silicon vacancy structures commonly referred to as carbon-antisite-vacancy pairs [44].

It is only when we compare spectrum B with A that the presence of the bistable *M* center becomes evident. The prominent peak at about 280 K in spectrum B is actually a superposition of $Z_{1/2}$ with M_2, the latter being converted to M_1 and M_3 in spectrum A (overlapping S_1 and S_2, respectively). As in Ref. [19], we find that above room temperature spectra A and B become identical as a result of the B → A transformation. This means that we do not have access to *M* center-related transitions deeper than M_3 (as it is expected for the location of M_4) by means of conventional DLTS.

Figure 2(b) depicts two isothermal DLTS spectra acquired sequentially at $T = 310$ K. Spectrum B was acquired first, after preannealing the sample at 450 K with no bias applied. During the 20-min recording time at $T = 310$ K, a large fraction of *M* centers was converted from configuration B to A. This could be confirmed from the loss of intensity of M_2 during subsequent identical measurements. Spectrum A was then recorded after warming up the sample at $T = 340$ K under reverse bias (−30 V) in order to reset all *M* centers to the A form. The isothermal signals have contributions from three groups of transients: A fast group with time constant $\tau \sim 10^{-1}$ s ($Z_{1/2}$ and M_2), an intermediate group with decay time of a few seconds (S_2 and M_3), and a slow group in the range $\tau \sim 10^2\text{–}10^3$ s (EH_4 and a new peak labeled M_4). The M_4 peak is clearly shown in the differential spectrum of Fig. 2(c). It has the same behavior of M_2 on annealing/biasing and corresponds to a trap concentration identical to that of M_1, M_2, and M_3 ($7\text{–}8 \times 10^{11}\,\mathrm{cm}^{-3}$).

From a fit of a T^2-corrected Arrhenius function to the M_4 data, we obtain an activation energy for electron emission of $E_a = 0.86 \pm 0.02$ eV and an extrapolated capture cross-section $\sigma_a = 4 \times 10^{-15}\,\mathrm{cm}^2$ which is coherent with a

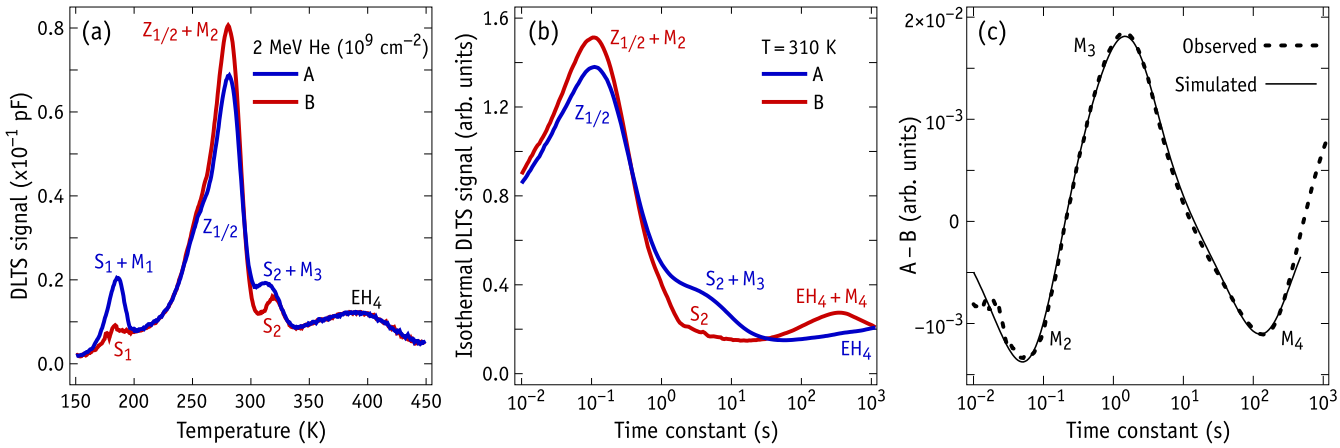

FIG. 2. (a) DLTS spectra of 2-MeV He implanted 4*H*-SiC SBD showing two configurations of the *M* center (A and B) along with other (labeled) deep traps. (b) Isothermal DLTS signals of the *M* center in configurations A (blue) and B (red) at 310 K. M_2, M_3, and M_4 overlap with $Z_{1/2}$, S_2 and EH_4, respectively. (c) Differential signal (dotted curve) of the isothermal spectra shown in (b). The thin solid line represents the simulated signal from M_2, M_3, and M_4 deep traps obtained by nonlinear fitting. See text for experimental details.

first acceptor transition. Although we could not directly measure the capture cross-section of M_4, the agreement with the calculated $C_i^-(k_a) \rightarrow C_i^0(k_c) + e^-$ transition energy of 0.92 eV is striking. Also notable is the agreement shown in Fig. 2(c) between the isothermal data (dotted line) and its theoretical counterpart (solid line) [41], obtained via nonlinear fitting constrained by the measured emission rates of M_2, M_3, and M_4.

Unfortunately, the measurements cannot discern whether M_4 is an evidence of (i) $B^- \rightarrow B^0 + e^-$ followed by $B^0 \rightarrow A^0$ or (ii) $B^- \rightarrow A^-$ immediately followed by $A^- \rightarrow A^0 + e^-$. The second and first steps of (i) and (ii), respectively, are necessary to explain the gradual conversion of B into A during the isothermal transients. The calculations account for $B^0 \rightarrow A^0$ in (i) if we consider the spin-flipping transition shown as a dashed line in the CCD. On the other hand, the first step of route (ii) has a measured activation energy of 0.9 eV, very close to the M_4 emission energy, and this could reflect the rate-limiting process toward A^0. Regarding the C_i model, although being consistent with both alternatives, this issue certainly calls for further clarification.

Another aspect that deserves a closer look concerns the annealing mechanism of the *M* center. The observed first-order kinetics suggests an annealing rate that depends on its own concentration only. A possible explanation stems from the indication that C_i defects are most likely negatively charged during annealing, thus being Coulomb-attracted by abundant nitrogen donors. The products of such reaction could be the EB centers reported by Beyer *et al.* [20].

The list of alternative defects, other than C_i, that could be related to the *M* center is not long. A Si displacement is unlikely, given that *M* was observed in material irradiated with electrons whose energy was below the necessary displacement threshold [20]. Further, we know that the Si self-interstitial is not an acceptor and has levels considerably deeper than those of M [40].

A stronger contender is a carbon Frenkel pair. Carbon vacancies and self-interstitials have electron traps deeper than $\sim E_c - 0.4$ eV. In n-type material they are both negatively charged, and Coulomb interactions between pairs with varying distances should lead to a strong dispersion of their respective trap depths. This effect is observed in DLTS spectra of as irradiated samples, but does not conform with the relatively clean M peaks, which are only visible after a gentle ($T \sim 200\,^\circ$C) annealing [30,45]. We investigated the stability of close Frenkel pairs and found a family of markedly low-energy structures. Their formation energy is in the range 5.5–6.5 eV, but the annihilation barrier is about 0.1–0.2 eV and therefore could not survive even at room temperature.

Based on first-principles calculations and junction spectroscopy, we provide substantial and credible arguments that allow us to conclude that the *M* center in 4*H*-SiC is a carbon self-interstitial. The observation of a new peak, labeled M_4 and possibly connected to a previously anticipated acceptor transition, provides an important piece of evidence in the connection between *M* and the interstitial. The model developed is summarized in Fig 1(a) in the form of a CCD. It incorporates the observed features of *M*, including charge states, bistability, annealing, reconfiguration kinetics, and electronic transition levels. The *M* center peaks are either "hidden" by the prominent $Z_{1/2}$ signal (carbon vacancy) or by $S_{1/2}$ (silicon vacancy) and $EH_{1/3}$ (unidentified). While this may explain the difficulty in the identification of C_i in n-type 4*H*-SiC, it certainly has undermined the interpretation of defect evolution by means of DLTS, in particular during annealing. The identification of the *M* center in 4*H*-SiC as the C_i defect will contribute to a better understanding of defect-related processes, ranging from self-diffusion to the activation and migration of dopants and impurities introduced by ion-implantation.

This work was supported by the NATO SPS Programme through Project G5674. J.C. thanks the FCT in Portugal for support through Projects UIDB/50025/2020, UIDP/50025/2020, and CPCA/A0/7277/2020 (Advanced Computing Project using the Oblivion supercomputer). J.D.G. acknowledges the support of I3N through Grant BPD-11(5017/2018). T.O. thanks Dr. Hidekazu Tsuchida and Dr. Norihiro Hoshino at CRIEPI for growing the 4*H*-SiC epitaxial layers. Z.P. acknowledges the financial support of the Australian Government to the CAS of ANSTO through the NCRIS.

[1] T. Kimoto and J. A. Cooper, *Fundamentals of Silicon Carbide Technology: Growth, Characterization, Devices and Applications* (Wiley, Singapore, 2014).

[2] X. She, A. Q. Huang, O. Lucia, and B. Ozpineci, IEEE Trans. Indust. Electronics **64**, 8193 (2017).

[3] J. R. Weber, W. F. Koehl, J. B. Varley, A. Janotti, B. B. Buckley, C. G. V. de Walle, and D. D. Awschalom, Proc. Natl. Acad. Sci. USA **107**, 8513 (2010).

[4] W. F. Koehl, B. B. Buckley, F. J. Heremans, G. Calusine, and D. D. Awschalom, Nature (London) **479**, 84 (2011).

[5] V. Ivády, J. Davidsson, N. Delegan, A. L. Falk, P. V. Klimov, S. J. Whiteley, S. O. Hruszkewycz, M. V. Holt, F. J. Heremans, N. T. Son, D. D. Awschalom, I. A. Abrikosov, and A. Gali, Nat. Commun. **10**, 5607 (2019).

[6] S. Castelletto and A. Boretti, J. Phys.: Photonics **2**, 022001 (2020).

[7] N. T. Son, X. T. Trinh, L. S. Løvlie, B. G. Svensson, K. Kawahara, J. Suda, T. Kimoto, T. Umeda, J. Isoya, T. Makino, T. Ohshima, and E. Janzén, Phys. Rev. Lett. **109**, 187603 (2012).

[8] X. T. Trinh, K. Szász, T. Hornos, K. Kawahara, J. Suda, T. Kimoto, A. Gali, E. Janzén, and N. T. Son, Phys. Rev. B **88**, 235209 (2013).

[9] I. Capan, T. Brodar, Z. Pastuović, R. Siegele, T. Ohshima, S.-i. Sato, T. Makino, L. Snoj, V. Radulović, J. Coutinho, V. J. B. Torres, and K. Demmouche, J. Appl. Phys. **123**, 161597 (2018).

[10] N. T. Son, P. Stenberg, V. Jokubavicius, T. Ohshima, J. U. Hassan, and I. G. Ivanov, J. Phys.: Condens. Matter **31**, 195501 (2019).

[11] R. K. Defo, X. Zhang, D. Bracher, G. Kim, E. Hu, and E. Kaxiras, Phys. Rev. B **98**, 104103 (2018).

[12] P. Udvarhelyi, G. Thiering, N. Morioka, C. Babin, F. Kaiser, D. Lukin, T. Ohshima, J. Ul-Hassan, N. T. Son, J. Vučković, J. Wrachtrup, and A. Gali, Phys. Rev. Appl. **13**, 054017 (2020).

[13] M. E. Bathen, A. Galeckas, J. Müting, H. M. Ayedh, U. Grossner, J. Coutinho, Y. K. Frodason, and L. Vines, npj Quantum Inf. **5**, 111 (2019).

[14] T. Hiyoshi and T. Kimoto, Appl. Phys. Express **2**, 041101 (2009).

[15] L. S. Løvlie and B. G. Svensson, Appl. Phys. Lett. **98**, 052108 (2011).

[16] C. Hemmingsson, N. T. Son, O. Kordina, J. P. Bergman, E. Janzén, J. L. Lindström, S. Savage, and N. Nordell, J. Appl. Phys. **81**, 6155 (1997).

[17] G. Alfieri and A. Mihaila, J. Phys.: Condens. Matter **32**, 465703 (2020).

[18] D. M. Martin, H. Kortegaard Nielsen, P. Lévêque, A. Hallén, G. Alfieri, and B. G. Svensson, Appl. Phys. Lett. **84**, 1704 (2004).

[19] H. K. Nielsen, A. Hallén, and B. G. Svensson, Phys. Rev. B **72**, 085208 (2005).

[20] F. C. Beyer, C. Hemmingsson, H. Pedersen, A. Henry, E. Janzén, J. Isoya, N. Morishita, and T. Ohshima, J. Appl. Phys. **109**, 103703 (2011).

[21] M. Bockstedte, A. Mattausch, and O. Pankratov, Phys. Rev. B **68**, 205201 (2003).

[22] A. Gali, P. Deák, P. Ordejón, N. T. Son, E. Janzén, and W. J. Choyke, Phys. Rev. B **68**, 125201 (2003).

[23] T. Kobayashi, K. Harada, Y. Kumagai, F. Oba, and Y. ichiro Matsushita, J. Appl. Phys. **125**, 125701 (2019).

[24] H. Itoh, A. Kawasuso, T. Ohshima, M. Yoshikawa, I. Nashiyama, S. Tanigawa, S. Misawa, H. Okumura, and S. Yoshida, Phys. Sstatus Solidi A **162**, 173 (1997).

[25] N. T. Son, P. Hai, and E. Janzén, Mater. Sci. Forum **353–356**, 499 (2001).

[26] T. T. Petrenko, T. L. Petrenko, and V. Y. Bratus, J. Phys.: Condens. Matter **14**, 12433 (2002).

[27] U. Gerstmann, A. P. Seitsonen, D. Ceresoli, F. Mauri, H. J. von Bardeleben, J. L. Cantin, and J. Garcia Lopez, Phys. Rev. B **81**, 195208 (2010).

[28] J. Lefèvre, J.-M. Costantini, S. Esnouf, and G. Petite, J. Appl. Phys. **105**, 023520 (2009).

[29] C. G. Hemmingsson, N. T. Son, A. Ellison, J. Zhang, and E. Janzén, Phys. Rev. B **58**, R10119(R) (1998).

[30] M. L. David, G. Alfieri, E. M. Monakhov, A. Hallén, C. Blanchard, B. G. Svensson, and J. F. Barbot, J. Appl. Phys. **95**, 4728 (2004).

[31] P. E. Blöchl, Phys. Rev. B **50**, 17953 (1994).

[32] G. Kresse and J. Furthmüller, Comput. Mater. Sci. **6**, 15 (1996).

[33] G. Kresse and J. Furthmüller, Phys. Rev. B **54**, 11169 (1996).

[34] J. Heyd, G. E. Scuseria, and M. Ernzerhof, J. Chem. Phys. **118**, 8207 (2003).

[35] J. P. Perdew, K. Burke, and M. Ernzerhof, Phys. Rev. Lett. **77**, 3865 (1996).

[36] G. Henkelman, B. P. Uberuaga, and H. Jónsson, J. Chem. Phys. **113**, 9901 (2000).

[37] C. Freysoldt, B. Grabowski, T. Hickel, J. Neugebauer, G. Kresse, A. Janotti, and C. G. van de Walle, Rev. Mod. Phys. **86**, 253 (2014).

[38] C. Freysoldt, J. Neugebauer, and C. G. Van de Walle, Phys. Rev. Lett. **102**, 016402 (2009).

[39] M. E. Bathen, J. Coutinho, H. M. Ayedh, J. UI Hassan, I. Farkas, S. Öberg, Y. K. Frodason, B. G. Svensson, and L. Vines, Phys. Rev. B **100**, 014103 (2019).

[40] J. Coutinho, Crystals **11**, 167 (2021).

[41] Y. Tokuda, N. Shimizu, and A. Usami, Jpn. J. Appl. Phys. **18**, 309 (1979).

[42] Y. Tokuda, J. Appl. Phys. **100**, 023704 (2006).

[43] D. C. Hunt, D. J. Twitchen, M. E. Newton, J. M. Baker, T. R. Anthony, W. F. Banholzer, and S. S. Vagarali, Phys. Rev. B **61**, 3863 (2000).

[44] R. Karsthof, M. E. Bathen, A. Galeckas, and L. Vines, Phys. Rev. B **102**, 184111 (2020).

[45] J. P. Doyle, M. K. Linnarsson, P. Pellegrino, N. Keskitalo, B. G. Svensson, A. Schöner, N. Nordell, and J. L. Lindström, J. Appl. Phys. **84**, 1354 (1998).